Experimental and numerical investigation of the unclogging process within propped fractures using dynamic stimulation

Fawaz Youssef, Christian La Borderie, Antoine Jacques, Gilles Pijaudier-Cabot

OPEN GEOMECHANICS

Experimental and numerical investigation of the unclogging process within propped fractures using dynamic stimulation

Fawaz Youssef [a, b], *Christian La Borderie* [c], *Antoine Jacques* [d] & *Gilles Pijaudier-Cabot* [a, e]

[a] *Univ. de Pau et des Pays de l'Adour, CNRS, Total, LFCR, Anglet, France*

[b] *Andra, Meuse/Haute-Marne Underground Research Lab., Bure, France*

[c] *Univ.de Pau et des Pays de l'Adour, SIAME, Anglet, France*

[d] *TotalEnergies E&P, CSTJF, Pau, France*

[e] *Institut Universitaire de France, Anglet, France.*

Published
13th June 2024
https://doi.org/10.5802/ogeo.19

Edited by
Chloé Arson
Civil and Environmental Engineering
Cornell University
Ithaca, NY 14853, USA

Reviewed by
Derek Elsworth
Pennsylvania State University
Pennsylvania, USA
An second reviewer
(anonymous)

Correspondence
Fawaz Youssef
Univ. de Pau et des Pays de l'Adour,
CNRS, Total, LFCR, Anglet, France
Andra, Meuse/Haute-Marne
Underground Research Lab., Bure,
France
Centre de Meuse / Haute-Marne
(CMHM)
Route départementale 960- BP 9 – 55290
Bure, France
youssef.fawaz@univ-pau.fr

Open Geomechanics is member of the
Centre Mersenne for Open Scientific Publishing

Abstract. Dynamic excitation of reservoir systems trapping hydrocarbons is a potentially promising solution for increasing the production. At the laboratory scale, it was found that a vibration of the fluid pressure could induce an increase in permeability of fractures. We developed in a previous study experiments aimed at reproducing clogging in propped fractures and unclogging due to dynamic loads applied perpendicularly to the fracture [Fawaz et al., 2021]. This paper built on this experimental set-up and presents first a study of the major parameters governing the unclogging of propped fractures by dynamic stimulation. The influences of the quantity of fine particles clogging the fracture, amplitude and frequency of the signal are investigated at constant proppant density. Then, a prototype computational model based on coupled DEM and finite volume method is developed. An original formulation of the evolution of apparent permeability of the fracture due to the presence and motion of solid particles in each finite volume cell is presented. Computations are consistent with experiments, although axial fluid flow is modelled instead of radial flow in the experiments. Results show that the increase of fracture conductivity is strongly related to the movement of proppant which helps at releasing and destabilizing fines clusters.

Keywords. Fracture, proppant, stimulation, dynamic stressing, unclogging, intrinsic permeability, DEM

1. Introduction

Increasing hydrocarbon production, or heat production in geothermal applications, is strongly related to the status of the fracture network existing in the geological formation that hosts the fluids to be extracted and/or injected. One of the main parameters in characterizing reservoirs is the hydraulic conductivity of these fractures.

Hydraulic fracturing is an effective method for increasing the reservoir's hydraulic conductivity [Economides and Nolte, 2000]. This method involves driving cracks in the reservoir rock mass with a proppant-loaded fluid injected at high pressure. The proppant's primary function is to prevent the fracture from closing after the fluid pressure has been released, and therefore to guarantee that fracture will have a sufficiently high conductivity.

However, propped fractures can be damaged over time due to the presence of fine particles [Bennion, 2002]. These fine particles result from fracture walls degradation [Reinicke et al., 2010], proppant crushing [Bedrikovetsky et al., 2012], and drilling and completion operations fluids [Kang et al., 2014]. They can also result from the incompatibility between the fluids used (for stimulation, completion, drilling…) and the rock reservoir [Chen et al., 2010, Kang et al., 2014, Xu et al., 2016] and form organic and inorganic scales (i.e., Barite, Calcite…). This leads to a decrease of the conductivity of the fracture network, and also to a drastic drop in hydrocarbon production or fluid injectivity.

To remedy this issue, EOR operations or chemical stimulation (i.e., acidizing…) are implemented to rejuvenate the well production. These operations intend to dissolve scales and fines. While these chemical methods have an effect that remains quite localized [Beresnev and Johnson, 1994, Kang et al., 2014], e.g. cleaning up production liners and zones near the wellbore, pore pressure oscillations may be a very good candidate to restore the permeability of fractures farther from the wellbore [Beresnev and Johnson, 1994, Nikolaevskiy et al., 1996]:

- It was demonstrated at the laboratory scale that oscillations of the pore pressure could improve the flow and the drainage system [Candela et al., 2015, Elkhoury et al., 2011, Manga et al., 2012, Roberts, 2005]. Propped fractures were not considered, however.
- [Fawaz et al., 2021] noticed that Rayleigh waves generated by fluid pressure bursts in the well could propagate along fracture at very long distances without attenuation.

Pore pressure oscillations may be applied directly during the injection of fluid but they will be attenuated.

Pore pressure oscillations may be also generated by the relative motion of the fracture surface due to Rayleigh waves under reservoir pressure, thereby enabling the stimulation on long distances without attenuation. It is this second solution that is envisioned here, opening the path to the stimulation of existing fractures far from the wellbore, without the need to control the fluid flow in the fracture system.

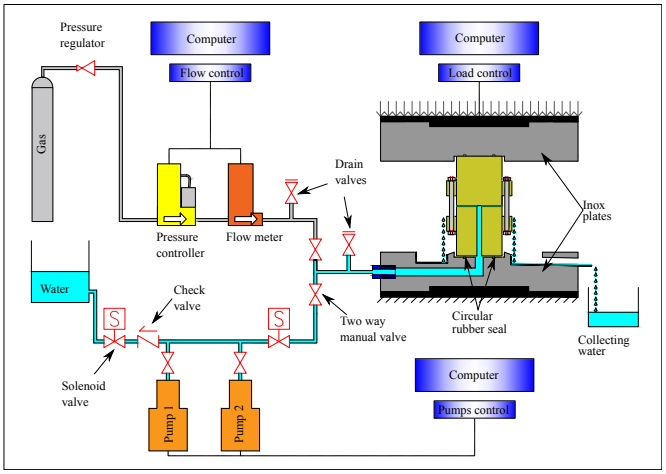

Figure 1. Experimental apparatus of the study [Fawaz et al., 2021]

The development of such a stimulation technique pointed out, among other practical challenges (see [Fensky et al., 2022]), the need to perform experiments on synthetic propped fractures to achieve a better appraisal of the influence of dynamic stimulation on the conductivity of propped fractures. This motivated the experiments developed by [Fawaz et al., 2021] where unclogging of a clogged propped fracture subjected to dynamic stressing was successfully reproduced in the laboratory. The intrinsic permeability of clogged fractures was increased showing a high recovery of the initial permeability. X-ray studies helped at checking that indeed dynamic loading induced a motion of clusters of fine particles that were initially blocked between proppant. The parameters governing the unclogging process were the proppant distribution density, the proppant granulometry, the quantity of clogging materials, the amplitude, frequency, and shape of the dynamic signal.

The purpose of this paper is twofold: first, we investigate the parameters that control unclogging experimentally, considering a fixed amount of proppant in the fracture; second, we discuss a prototype numerical model that is aimed at understanding the basic local mechanisms that are at stake during the unclogging process.

We begin with a brief description of the experimental method presented in [Fawaz et al., 2021]. In Section 3, experimental results are discussed. Section 4 is dedicated to the computational model. Comparisons with some experiments are presented. It is found that an important mechanism that controls the unclogging process is the motion of proppant particles during the stimulation, that helps to destabilize clusters of fine particles.

2. Experimental method

2.1. Set-up

Experiments are performed on an artificially propped fracture using the apparatus in Figure 1. The propped annular fracture is located at the middle of a cylinder made of polycarbonate. The full specimen is composed of two cylindrical samples with an outer diameter of $D = 46\,\text{mm}$

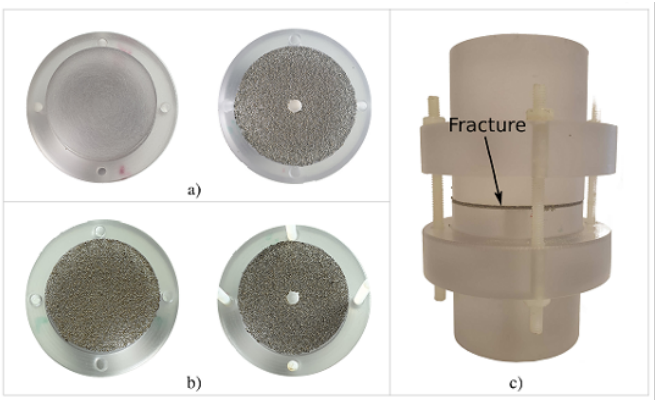

Figure 2. Specimen preparation procedure (building the propped fracture): a) distribution of a single proppant layer on the lower polycarbonate sample; b) distribution of doubled proppant layer on both polycarbonate samples; c) Fracture filled with two proppant layers after installing a fixing system (nylon rods and nuts)[Fawaz et al., 2021].

and a height of $H = 50\,\text{mm}$ (Figure 2). The bottom one has a borehole of $d = 6\,\text{mm}$ where the fluid is injected. The space between both parts of the sample is filled with proppant and the fluid flows radially.

Permeability is measured by the radial circulation of the fluid in the fracture, injected in the borehole of the lower part of the specimen. At the same time, the specimen is loaded axially. Static loads represent the vertical geological stress applied on the fracture, and dynamic loads are superimposed to this base signal in order to stimulate the fracture. A uniaxial servo-hydraulic press is used to apply both dynamic and static loads. Two circuits are used to ensure permeability measurement: a series of 2 pumps (max flowrates: 16.28 mL/min & 240 mL/min) that measure the flow and pressure of water. For gas measurements, we use a mass flowmeter, a pressure regulator, and a backpressure controller. The permeability measurements are performed under static uniaxial stress of 20 MPa (34 kN) to mirror the geological constraints.

Darcy's law is used to determine the intrinsic permeability at a steady viscous flow regime. The pump with lower maximum flowrate (16.38 mL/min) is used to measure the intrinsic permeability at a flowrate of 8.8 mL/min. Derived from Darcy's law, the water intrinsic permeability K_w in a radial flow is obtained as follow:

$$K_w = \frac{\mu \ln(\frac{R_2}{R_1}) Q}{2\pi h (P_1 - P_2)} \tag{1}$$

where μ is the dynamic viscosity of freshwater (10^{-3} Pa.s), R_1 is the radius of the inner borehole of the bottom sample (3 mm), R_2 is the outer radius of the bottom sample (23 mm), Q is the upstream flow rate (~8.8ml/min), h the fracture opening (~0.58-0.9 mm), P_1 the inlet pressure (which varies according to the state of the fracture) and P_2 the outlet atmospheric pressure.

Moving to the gas permeability measurements, the apparent permeability K_{aG} is obtained according to the following formula:

$$K_{aG} = \frac{\mu \ln(\frac{R_2}{R_1}) Q P_2}{\pi h (P_1^2 - P_2^2)} \tag{2}$$

where μ is here the dynamic viscosity of gas (nitrogen, 1.76×10^{-5} Pa.s). The propped fracture has a high permeability to gas (high seepage velocity) and therefore, the flow tends to be unsteady, non-linear and inertial. As detailed in [Fawaz et al., 2021], the Forchheimer approach is used. The intrinsic permeability K_{in} is then determined after measuring the apparent permeability K_{aG} at many various inlet pressures. Intrinsic permeabilities of the propped fracture, as obtained from water and gas measurements, are similar.

Experimentally, one has access to the global flow rate in the fracture, and to the inlet and outlet pressures. Inside the propped fracture, it is expected that due to the fines and proppant distribution, preferential flow paths may form and evolve during the dynamic stimulation (as we will see in Section 4). Preferential flow paths break the axisymmetric flow, and local flow rates and pressures are thus expected to be quite different from those assumed for the derivation of eq. (1), eq. (2). These equations are approximates that serve at the derivation of an equivalent homogeneous permeability from global quantities.

In the foregoing, we will show the evolutions of this (intrinsic) equivalent homogeneous permeability, although we refer to "permeability", for the sake of brevity. This quantity may be used in eq. (1), eq. (2) to convert all permeability results into the evolution of the global flow rate due to clogging/unclogging.

2.2. Preparation of the samples

Two sizes of proppant are used: proppant 40/70 and proppant 30/50. The particle size distribution of both proppants is presented in Figure 3c. Figure 3a and Figure 3b show the particle size analysis of the 30/50 and 40/70 proppants used according to US standards.

Throughout this experimental study, results are shown for fractures filled with 2 layers of proppant where the distribution density is 800-1200 g/m^2. This is twice the maximum density of proppant placed on a single unit surface in a single layer (the methodology described in [Fawaz et al., 2021] is followed). After the specimen has been obtained, it is introduced under the hydraulic jack between two inox plates and loaded up to the reference stress of 20 MPa. Then, gas and water permeability measurements are performed.

The next step consists in clogging the propped fracture. The fracture is opened again and then spread with different amounts of natural crushed sand (25µm-75µm) (see [Fawaz et al., 2021] for details). In this study, the size distribution of the fine particles has been kept constant. As we will see in the discussion of the experimental results, there is no doubt, however, that it should play a role on the clogging/unclogging process.

Fractures filled with proppant 40/70 were clogged with 5 %, 10 %, and 15 % of fines (mass of fines divided by the mass of proppant), and fractures filled with proppant 30/50

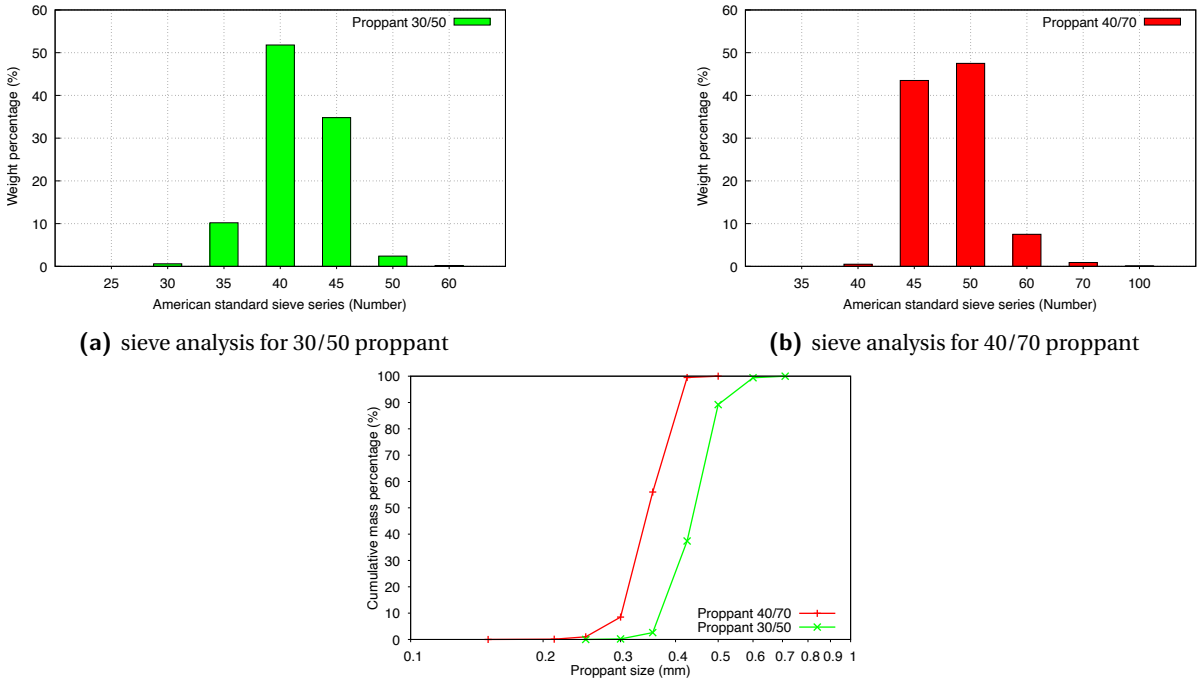

(a) sieve analysis for 30/50 proppant

(b) sieve analysis for 40/70 proppant

(c) Particle-size distributions of both proppants

Figure 3. Proppant granulometry (Weight percentage according to sieve series numbers)

were clogged with 15 %, 25 %, 35 %, and 45 % of fines. After closing the fracture, the axial load is applied again and water injection is performed to block fines in the proppant medium. Water and gas permeabilities of the clogged fracture are measured again.

2.3. Dynamic stimulation

Unclogging is performed by applying cyclic uniaxial compression while holding the upstream water flow constant (240 mL/min). All the tests have been performed at the same flow rate. Same as for the size distribution of the fine particles, it is intuitively expected that the flow rate has an important effect (although it is not expected to be controlled in field applications). The higher it is, the lower clogging might be effective as fine particles may be flushed outside the specimen, without having the opportunity to form clusters and clog the fracture. Square signal oscillations are imposed during this process (Figure 4). Tests are performed with two frequencies of 1 Hz and 10 Hz, and two amplitudes of 2.7 MPa and 5.4 MPa. Table 1 provides all the parameters of the experiments.

During the dynamic stimulation, fines are further flushed out of the specimen and clusters of fine particles are destroyed (and may form again elsewhere in the fracture), as observed in [Fawaz et al., 2021] with the help of X-ray scans. It yields a decrease of the water injection pressure (because the flux is constant) and an increase of the hydraulic conductivity of the fracture. Once we reach a permanent regime with a constant pressure injection, the number of cycles is recorded, and the dynamic stimulation is stopped. Water and gas permeability are measured. The permeability recovery rate is computed. It is the ratio of the difference between

Table 1. Parameters of the experiments.

(a) Permeability

Parameters	Value	Description
Static stress	20 MPa	Stress at which the permeability is measured
water flow	8.8 mL/min	Water permeability (viscous flow)
outlet pressure	1 atm	Atmospheric pressure
Relative gas inlet pressure	0.1 – 2.5 bar	Gas permeability (inertial flow)

(b) unclogging process

Parameters	Value	Description
Water flow	240 mL/min	Used for the unclogging process
Frequency	1 Hz & 10 Hz	Dynamic stressing parameters:
Stress amplitude	±2.7 MPa ±5.4 MPa	square signal
Displacement of the jack	±0.125 mm ±0.25 mm	
Average stress	13.24 MPa	

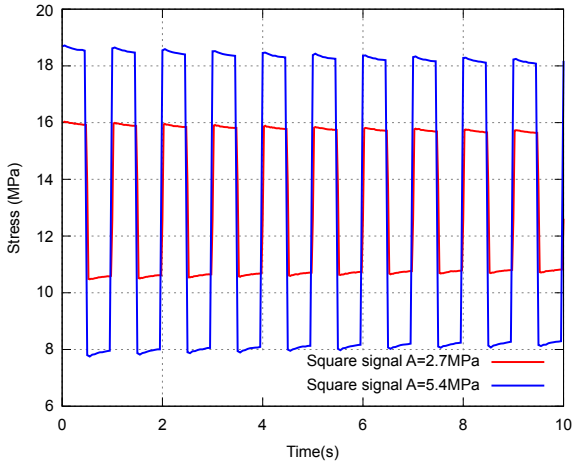

(a) $f = 1\,\text{Hz}$

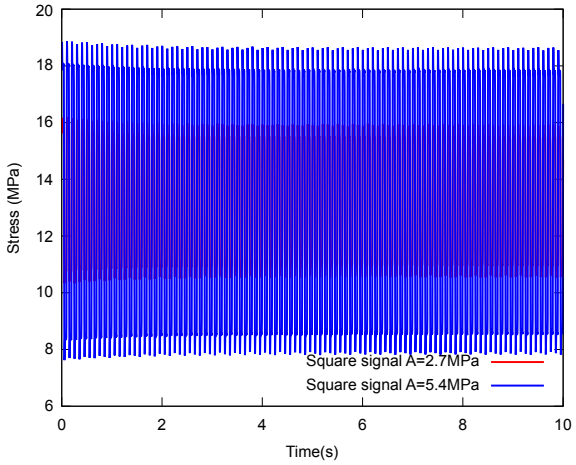

(b) $f = 10\,\text{Hz}$

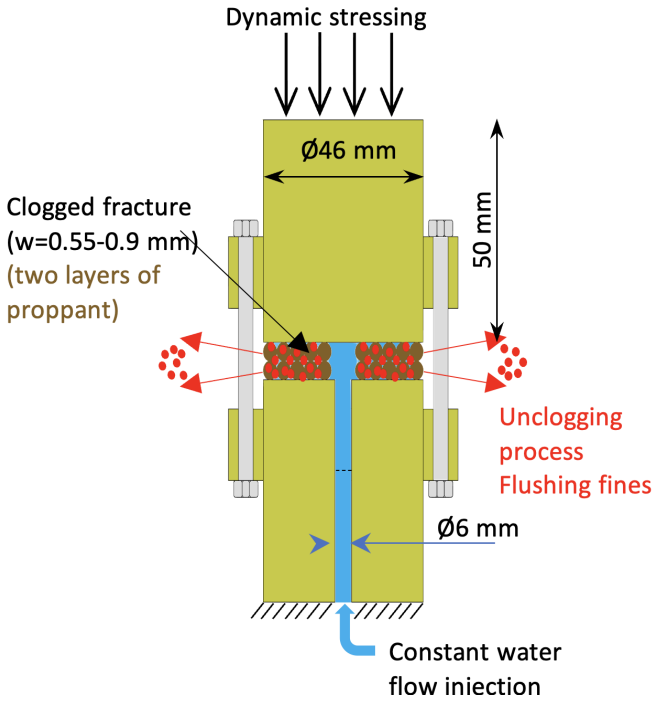

(c) Schematic description of the fluid flow in the propped fracture. Upon applying the dynamic loads with a constant flow injection, fines are flushed out from the fracture.

Figure 4. Characteristics of the dynamic stimulation: a), b) the experiments consist of imposing multiple sets of square signal oscillations using two amplitudes and two frequencies for the unclogging process ($A =$ 2.7 & 5.4 MPa, $f =$ 1 & 10 Hz)

the permeability of the stimulated fracture minus the permeability of the clogged fracture, divided by the difference between the initial permeability of the clean fracture minus that of the clogged fracture.

3. Experimental Results and Discussion

The present study focuses on the influence of the amplitude and frequency of the dynamic signal because it has been shown that they play a very important role in the natural fracture unclogging response [Beresnev et al., 2005, Candela et al., 2014, Elkhoury et al., 2011]. Fractures clogged with various quantities of fine particles are considered.

3.1. Influence of the quantity of fine particles

3.1.1. Proppant 40/70

To observe unclogging and to analyze the repeatability of the tests on fractures filled with 5 %, 10 %, and 15 % fines, three series of tests were performed with a dynamic square signal loading ($f = 1\,\text{Hz}$, $A = 5.4\,\text{MPa}$). Figure 5 shows the

result of the dynamic stimulation. The evolution of the permeability is plotted as a function of the number of pulses. The permeability is measured here directly during the evolution of the water injection pressure. In all cases, dynamic loading results in an increase of permeability. This evolution follows a nearly identical pattern in all the tests. It varies with the percentage of clogging fines. The permeability recovery rate observed in these tests varies between 12 % and 69 %. Fractures clogged with 5 % fines show a smaller recovery rate than those clogged with 10 and 15 % of fines. But on the other side, the permeability of clogged fractures decreases significantly as the quantity of fines increases. The percentage of fines lost at the end of these tests varies between 30 % and 65 %.

This confirms that it is indeed the motion of fine particles, flushed outside the fracture, that induces the increase of permeability. In these experiments, the geometry of the fluid flow and the size of the fracture play an important role. The gradient of pressure in the fracture depends on the geometry of the fracture (influenced most probably by preferential paths generated during unclogging). For larger specimens also, fines may further form clusters closer to the fluid outlet with little effect on the permeability. These effects could be further investigated using the numerical model devised in Section 4, once it is proved that it can capture the basic mechanisms involved during unclogging in the experiments.

Concerning the repeatability of the tests, the unclogging response is quite repeatable for a low quantity of fines (5 %). For 10 % of fine, the evolutions of permeability with the number of pulses can be also considered to be comparable, provided the permeability is normalized with the initial permeability. It is for the larger amount of fine that the tests exhibit the largest scattering. This may be due to the size of the specimen that might be too small and therefore quite sensitive to the creation of hydraulic paths with very high hydraulic conductivity.

A fourth percentage of fines (20 %) was tested with this proppant 40/70. Unclogging did not take place [Fawaz et al., 2021]. The permeability decreased slightly instead of increasing upon dynamic loading. We may consider in this case that the lack of efficiency of the stimulation was due to a dynamic signal that did not carry enough energy to unclog the fracture. Figure 6 presents the variation of the recovery rate and the number of pulses as a function of the percentage of clogging (% of fines) for these tests. With the least clogged fractures (i.e., 5 %) the permeability is quickly stabilized, which leads to a moderate recovery rate of 29 %. The number of pulses required is very low (150 to 370 pulses) compared to the other two tests performed with 10 and 15 % of fines. The recovery rate increases slightly (33 %) in the fractures clogged with 10 % of fines, followed by a significant increase (44 %) for those clogged with 15 % fines. This shows that the more the fracture is clogged, the higher the recovery rate, until reaching a clogging level that prevents unclogging for the considered dynamic signal. In our case, the maximal efficiency, for the given dynamic signal, is obtained for a clogging below 20 % of fines.

3.1.2. Proppant 30/50

Three series of tests were performed on fractures filled with two layers of proppant 30/50 under the same stimulation conditions. Since the particle size distribution of the proppant 30/50 is coarser than that of proppant 40/70 (in terms of particle diameter), it was possible to clog the fractures with higher percentages of fines (25 %, 35 %, and 45 %) compared to the tests with proppant 40/70. Results exhibit a stronger recovery of permeability upon unclogging for the same number of pulses compared to the tests with proppant 40/70 (Figure 7). The recovery rate for these tests varies between 38 % and 100 % with a remarkable loss of fines estimated between 71 % and 81 % at the end of the tests. The evolution of the recovery rates with the quantity of fines, reported in [Fawaz et al., 2021], is recalled in Figure 8. We observe that the number of pulses needed to achieve unclogging increases as the quantity of fine particles increases. This is a similar trend compared to that observed with proppant 40/70. As opposed to Figure 6, the recovery rate decreases as the quantity of fines increases.

The difference between the results with proppant 30/50 and 40/70 can be explained by comparing the proppant particle sizes to the size of the fine particles. The porosity of the proppant 30/50 is larger than that of the proppant 40/70, which induces an increase in the hydraulic diameter of the propped fracture. The average diameters of the proppants are: $D_{m40/70} = 0.34\,\text{mm}$ and $D_{m30/50} = 0.44\,\text{mm}$. If we take the case of a layer of proppant (worst case) to calculate the hydraulic diameter (see details in [Fawaz et al., 2021], the hydraulic diameter for the proppant 40/70 is $56\,\mu\text{m} < D_{h40/70} < 85\,\mu\text{m}$. For the proppant 30/50, the hydraulic diameter is $74\,\mu\text{m} < D_{h30/50} < 111\,\mu\text{m}$. Recall that the diameter of the fines varies between 25 µm and 75 µm. In the case of the proppant 40/70, fines with a diameter greater than 56 µm will be blocked in the porous matrix. With the proppant 30/50 and for a small quantity of fines, they can all be released enabling a quick recovery rate, close to 100 % at the end of the test. The recovery rate decreases necessarily as clusters of particles are formed for larger quantity of fines.

For proppant 40/70, a portion of fine particles remains blocked because they cannot pass in the pore throats. It is this relative quantity of blocked fine particles that controls the final permeability for low quantity of fines (and also for large quantities if we assume that all clusters are destroyed due to the stimulation). For larger quantities, clusters that form in between the proppant particles control the permeability in the clogged state. They are destabilized during the dynamic stimulation. The relative increase of permeability becomes greater than for low quantities of fine particles and the recovery rate increases eventually, as seen on Figure 6. These considerations highlight the influence of the relative sizes of fine and proppant particles.

3.2. Influence of the frequency

The four series of tests presented in Figure 9 show a peculiar aspect of the effect of frequency on the unclogging response. Fractures filled with two layers of proppant 30/50 and clogged with 15, 25, 35, and 45 %, were subjected to a

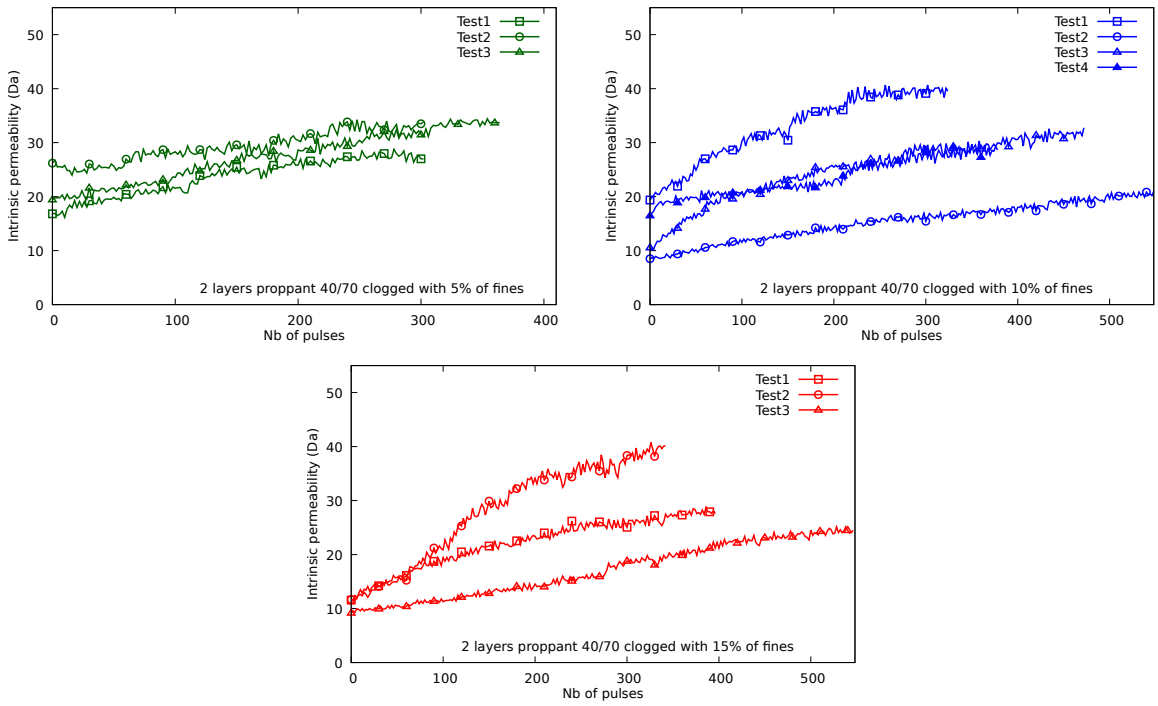

Figure 5. Evolution of the intrinsic permeability with three series of tests, using fractures filled with 2 layers of 40/70 proppant and clogged with 5, 10, 15 % of fines, subjected to a square signal loading (frequency $F = 1$ Hz, Amplitude $A = 5.4$ MPa).

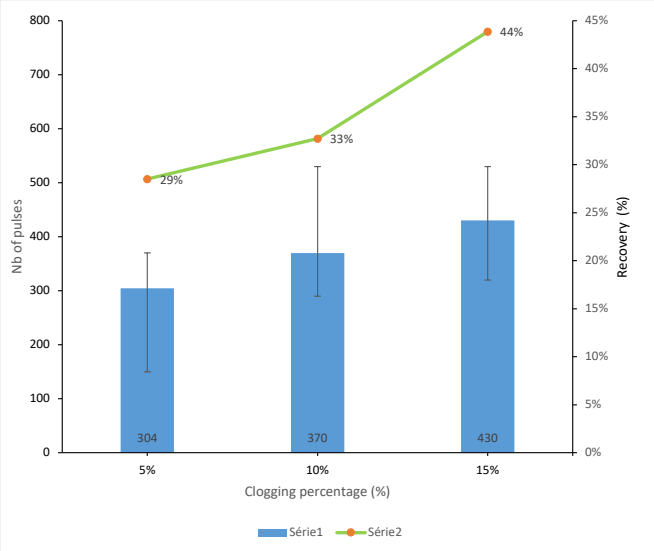

Figure 6. Variation of the recovery rate and the number of pulses required to obtain it as a function of the clogging percentages (two layers of 40/70 proppant, square dynamic signal of frequency $F = 1$ Hz and amplitude $A = 5.4$ MPa).

dynamic stressing with a square signal of frequencies 1 Hz and 10 Hz, and a constant amplitude of 2.7 MPa.

If we focus on the evolution of the permeability during stimulations performed with 1 Hz and 10 Hz, we find that with the less clogged fractures (15 %), the unclogging process with 1 Hz yields to a greater permeability recovery compared to the one performed with 10 Hz. The evolution of permeability curves at 1 Hz starts to approach that at 10 Hz in fractures clogged with 25 %. Above 25 % (i.e., 35 % and 45 %) one can notice the better efficiency of the highest frequency (10 Hz) compared to the lowest frequency (1 Hz).

As shown previously in section 3.1.2 we find also that the unclogging response is triggered at the beginning of the stimulation for 15 % and 25 % of fines. Moderate to higher clogged fractures (35 % and 45 %) show a delay in the unclogging response, where tests performed with a frequency of 10 Hz are faster than those performed with a frequency of 1 Hz. Figure 10 shows the corresponding evolutions of the recovery rates. The recovery rate of the tests performed with a frequency of 1 Hz varies between 7 % and 69 %, while for those performed with a frequency of 10 Hz varies between 9 % and 75 %. At a constant percentage of fines, increasing the frequency of dynamic loading results in an increase of recovery rates. The recovery rate decreases as the amount of fines increases (same as for the results in the previous section). A plateau can be noticed for a percentage of fines greater than 35 %, with very moderate recovery for the 1 Hz tests (13 %-15 %) and significant for the 10 Hz tests (31 %-39 %).

To summarize, increasing the frequency induces a significant increase of recovery rates when the quantity of fines is high, especially for 35 % and 45 % of fines. The number of pulses needed to achieve unclogging is smaller at low frequency than at high frequencies for low quantity of fines, but results are opposite for larger quantities of fines.

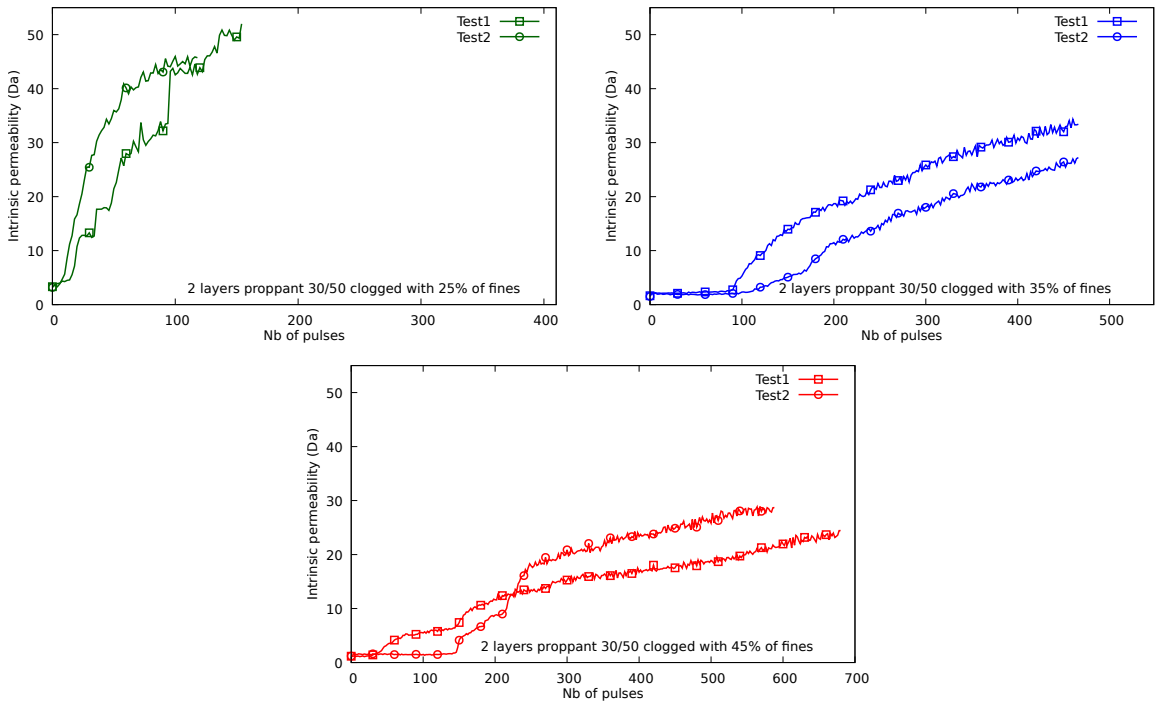

Figure 7. Evolution of the intrinsic permeability with three series of tests, using fractures filled with 2 layers of 30/50 proppant and clogged with 25 %, 35 %, 45 % fines subjected to a dynamic square signal loading ($F = 1$ Hz, $A = 5.4$ MPa).

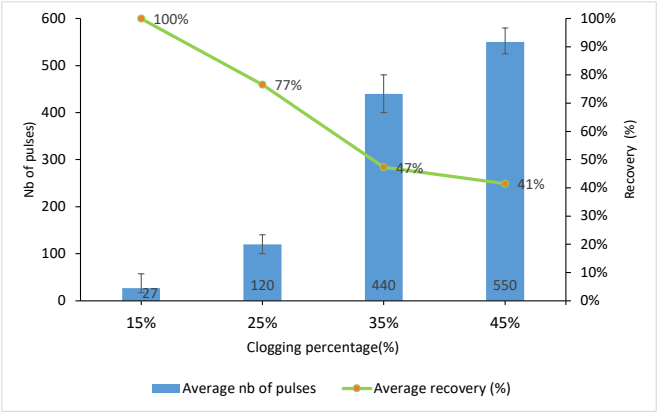

Figure 8. Variation of the recovery rate and the number of pulses required to obtain it as a function of the clogging percentages (two layers of 30/50 proppant, square dynamic signal of frequency $F = 1$ Hz and amplitude $A = 5.4$ MPa) [Fawaz et al., 2021].

Pressure oscillations induce drag forces on the fine particles. Fine particles will be set in relative motion with respect to the fluid and that should help at destabilizing clusters. For small quantities of fines, the quantity of clusters is expected to be small and they are easily destabilized at the beginning of the stimulation. The permeability recovery rate tends to be fast due to the removal of these clusters. It is the number of pulses that seems important. Then, fluid force oscillations applied in the fine particles and their frequency become then less effective because fines are gradually flushed out of the fracture. High frequencies are important when many clusters exist and form subsequently elsewhere after being destabilized. It is the collective effect of pressure oscillations at high frequency on clusters which becomes more effective when the quantity of fines is high. This is especially observed for dynamic stimulation at a low amplitude, which is the case here.

3.3. Influence of the amplitude

Now, we move to the study of the influence of the amplitude of the signal in fractures containing two layers of proppant 30/50, with a square signal of constant frequency (1 Hz) and two different amplitudes (2.7 MPa and 5.4 MPa). Figure 11 shows the results of the evolution of the permeability of the fractures clogged with 25 %, 35 %, and 45 %. We can notice that the unclogging response is more abrupt and effective for the stressing performed at amplitude 5.4 MPa compared to that of amplitude 2.7 MPa. For fractures containing 25 % fines, unclogging is triggered immediately after the application of the dynamic loading. The difference of increase of permeability achieved for the two amplitudes is detected for the moderate to higher clogged fractures (35 % and 45 %). In term of evolution of the permeability with the number of pulses, the response with 2.7 MPa lags behind that with 5.4 MPa by 150 pulses (35 % fine) and 650 pulses (45 %). These tests show a recovery rate that varies between 38 % and 100 % for an amplitude equal to 5.4 MPa, and between 7 % and 69 % for an amplitude equal to 2.7 MPa.

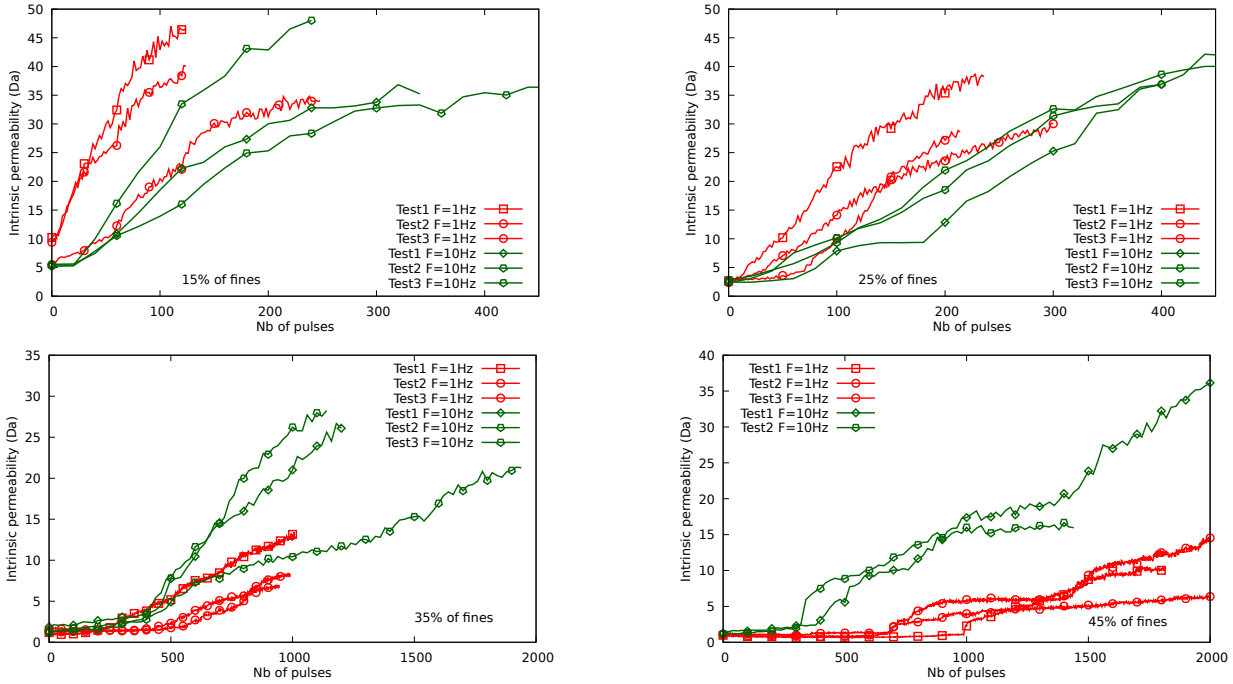

Figure 9. Influence of the frequency on the unclogging response: 4 series of tests of fractures filled with 2 layers of 30/50 proppant clogged with 15 %, 25 %, 35 %, 45 %, respectively (from left to right), with a square signal dynamic loading of ($F = 1$ Hz vs $F = 10$ Hz) of constant amplitude ($A = 2.7$ MPa).

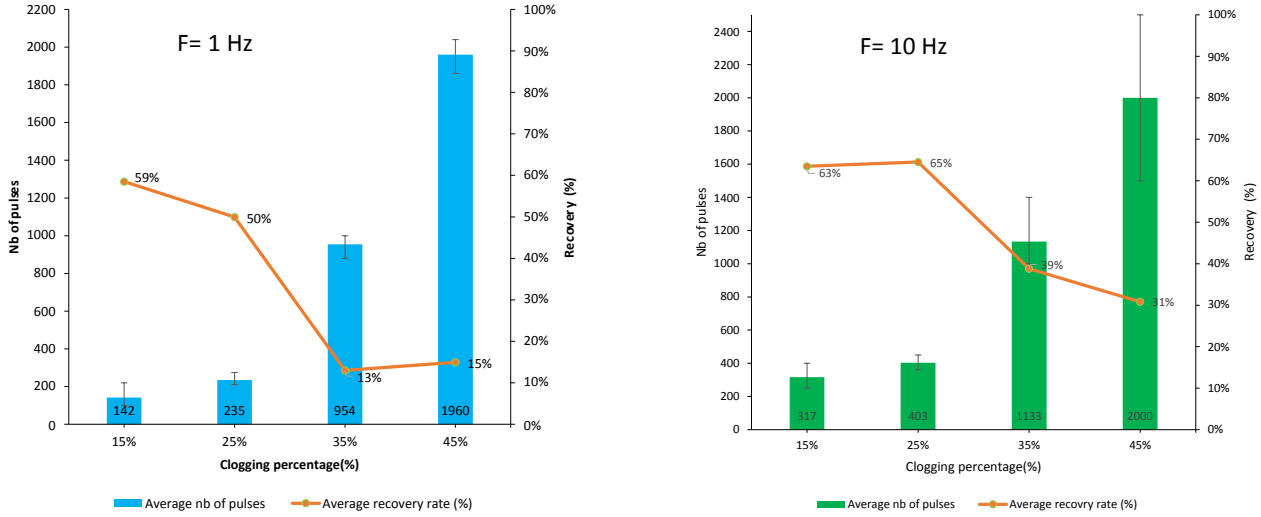

Figure 10. Summary: variation of the recovery rate and the number of pulses necessary to obtain it as a function of the clogging percentage (two layers of 30/50 proppant, square dynamic signal, $A = 2.7$ MPa) ;(a) $F = 1$ Hz, (b) $F = 10$ Hz.

Comparing Figure 11 and Figures 8 to 10, we observe similar trends. The recovery rate decreases with the increasing quantity of fines to reach a plateau. Yet, there are two differences: firstly, doubling the amplitude of the dynamic stressing (5.4 MPa) induces much higher recovery rates, and the plateau at which the recovery becomes constant increases from 15 % to about 40 %. Secondly, the number of pulses is increased by at least 50 % when the amplitude decreased (2.7 MPa); Therefore, using a high amplitude promotes a rapid unclogging process with a clear fracture cleaning as well.

Considering that the frequency of the stimulation acts on the motion of the fine particles and the destabilization of clusters essentially, one may infer that a possible explanation is that for high amplitudes, it is also the proppant particles that can be put into motion. It is then the conjunction of the destabilizing effect of pressure oscillations on clusters of fine particles and of the potential motion of proppant particles that accelerates the recovery of permeability. The higher the amplitude, the higher the pressure oscillations and the easier the motion of proppant particles.

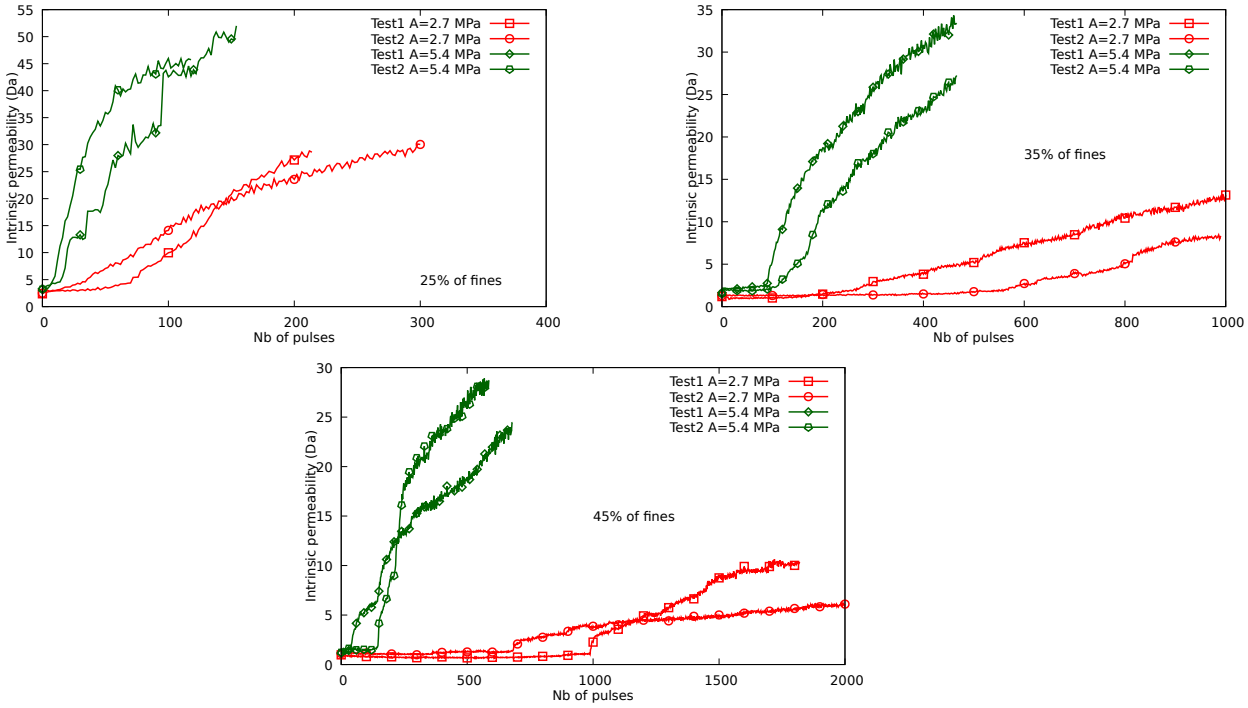

Figure 11. Influence of the amplitude on the unclogging response: 3 series of tests of fractures filled with 2 layers of 30/50 proppant clogged with 25 %, 35 %, and 45 %, respectively, with a dynamic loading having a square signal ($F = 1$ Hz vs $F = 10$ Hz, constant amplitude $A = 2.7$ MPa).

4. Computational model and comparisons

Computational modelling is expected to help at achieving a better understanding of the basic mechanisms at stake in the unclogging process under dynamic stimulation. We present here a prototype computational model for this purpose. It does not represent exactly the experimental conditions, yet the consistent comparisons with the measured data lend some confidence at unravelling the main mechanism that govern unclogging, namely destabilization of clusters of fine particles and motion of proppant particles.

The computational model bears several characteristics: (i) a discrete description of the proppant and fine particles, (ii) the simulation of the fluid flow and at the same time of the motion of the two faces of the propped fracture due to the dynamic stimulation, and (iii) a proper description of the coupled effect between the fluid and the solid particles. In the foregoing, we are going to implement a discrete element method for the proppant and fine particles, coupled to a finite volume calculation for the fluid part. This type of computational model stands among the standard features of the DEM code PFC3D [Itasca, 2018] used in the present study. The difficulty lies in capturing coupled effects: the effect of the fluid on the solid particles and the effect of the particle motion on the permeability. It is this second aspect for which we developed a new approach.

4.1. The DEM model

In the DEM model, the two faces of the propped fracture are modelled as two parallel planes. First the proppant particles are placed by gravity on one fracture surface. The interaction between the proppant particles and between the proppant particles and the surface of fracture follows the Hertz contact model (see Table 2). This is further particularly useful if one wants to mimic proppant embedment under load. The placement of proppant particles is obtained after equilibrium has been reached. Then the second plane (fracture surface opposite to the one on which the particles have been placed) is set.

A static uniaxial compression load is applied on the fracture planes in order to reach the geological axial stress of 20 MPa on the fracture. As an example, Figure 12 shows the case of a fracture filled with 0.5 layer of proppant 40/70. In this example, and further, the size of the numerical model is 8 mm × 10 mm. We have checked in each computation that the aperture of the fracture under load was similar to that measured in the experiments. Here it is 0.29 mm, very close to the measured one during the experiments (0.28 mm). In fact, the contact properties between the fracture planes and the proppant particles have been adjusted for this purpose.

In a second step, the fine particles are introduced in the numerical model. They are randomly placed in a portion of the fracture. Then, fluid flow is introduced to generate clusters and clogging (the fluid solid interactions will be described next).

Figure 13 illustrates this clogging process for a fracture filled with 0.5 layer of proppant 40/70. It is noteworthy that fine particles may leave the fracture in this process, when the

Table 2. Mechanical characteristics of the materials in the DEM model.

Parameters	Value
Fracture surface	
Young's modulus	2.3 GPa
Poisson coefficient	0.3
Friction coefficient μ	0.25
Proppant particles	
Density	2800 kg/m^3
Young's modulus	70 GPa
Poisson coefficient	0.23
Friction coefficient μ	0.25
Local damping coefficient	0.4
Fine particles	
Density	2650 kg/m^3
Effective contact stiffness	0.3 MPa
Friction coefficient μ	1.2
Local damping coefficient	0.8
Rolling resistance coefficient μ_r	1.2
Normal critical damping ratio β_n	0.2
Shear critical damping ratio β_s	0.2
Ratio of $\frac{K_n}{K_s}$	2

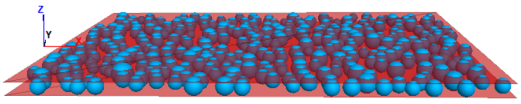

Figure 12. Fracture filled with 0.5 layer of proppant 40/70.

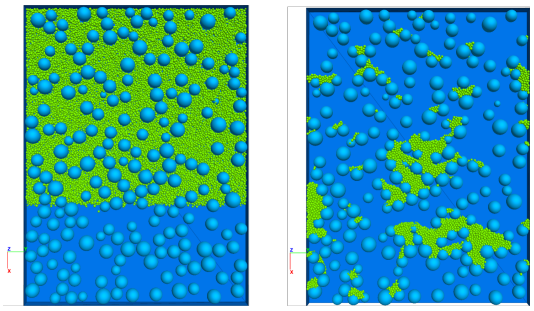

Figure 13. Fracture filled with 0.5 layer of proppant 40/70 – placement of fine particles before fluid flow (left) and after fluid flow (right).

density of proppant is not high especially. This is, however, also observed in the experiments.

Finally, the dynamic stimulation is applied by moving the upper and lower fracture surfaces according to sinusoidal functions with opposite phases, under load control. The frequencies correspond to those in the experiments and the total amplitude of the applied forces on the fracture corresponds to what is imposed during the experiments. Note that the shape of the dynamic signal in the computations is not the same as that used in the experiments. Experimentally, square signals are slightly more efficient than sinusoidal ones.

4.2. The fluid model

The fluid model is superimposed onto the DEM model. It is based on a classical finite volume method that solves for the velocity of the fluid phase within the propped fracture, seen as an equivalent homogenized medium with variable permeability depending on the presence of particles [Guyer et al., 2009]. A Python routine developed by Itasca was used to solve the fluid problem. In all our calculations, there is only one finite volume cell over the thickness of the propped fracture. In plane fluid motion is considered only. The discretization is regular: 32 by 16 cells over the fracture model (10 mm × 8 mm). The cell size is larger than the maximum proppant particle size (see the size distributions in Figure 3. It is much larger than the size of fine particles. Calculations are performed under the same conditions as in the experiments (fixed fluxes of fluid). Note that in the present calculations, mean fluid flux is axial whereas it is radial in the experiments.

The important ingredient in this model is the permeability of the fracture that is going to be used in Darcy's equation. This issue will be detailed in the next section.

4.3. Solid-fluid interactions

A staggered scheme has been implemented to achieve the coupling between the fluid model and the particle mechanical model. Influence of the fluid flow in the solid particles The forces applied on each particle are the contact forces, the inertia forces and the force due to the fluid flow. The latter, which is of interest here, is denoted as $\vec{f}_{fluid}$. It can be decomposed into three components:

$$\vec{f}_{fluid} = \vec{f}_{drag} + \vec{f}_{\nabla p} + \vec{f}_b \tag{3}$$

where $\vec{f}_{drag}$ is the drag force, $\vec{f}_{\nabla p}$is the force induced by the gradient of fluid pressure, and $\vec{f}_b$ is the buoyancy force. The expression of the drag force implemented in PFC3D is [Di Felice, 1994, Xu and Yu, 1997]:

$$\vec{f}_{drag} = \vec{f}_0\, \epsilon^{-X} \quad \text{with} \quad \vec{f}_0 = \frac{1}{2}\, C_d\, \rho_f\, \pi\, r^2\, |\vec{u} - \vec{v}|\, (\vec{u} - \vec{v}) \tag{4}$$

with ϵ the porosity of the cell (interparticle voids divided by the total volume of the cell), C_d the drag coefficient, ρ_f the mass density of the fluid, r the radius of the particle, $\vec{u}$ and $\vec{v}$ the velocity of the particle and of the fluid, respectively. ϵ^{-X} is factor that account for the average porosity of the cell in which the particle is located and inter-particle effects. The drag coefficient is:

$$C_d = 0.63 + \frac{4.8}{\sqrt{Re_P}} \quad \text{with} \quad Re_P = \frac{2.\rho_f.r.|u - v|}{\mu} \tag{5}$$

where Re_P is a "particle" Reynolds number and μ is the dynamic viscosity of the fluid. X in eq. (4) is empirically defined as:

$$X = 3.7 - 0.65\, e^{\left(-\frac{(1.5 - \log_{10} Re_P)}{2}\right)} \tag{6}$$

Adding the pressure gradient and buoyancy terms, one obtains:

$$\vec{f}_{fluid} = \vec{f}_{drag} + \frac{4}{3}\pi r^3 (\vec{\nabla} p - \rho_f \vec{g}) \tag{7}$$

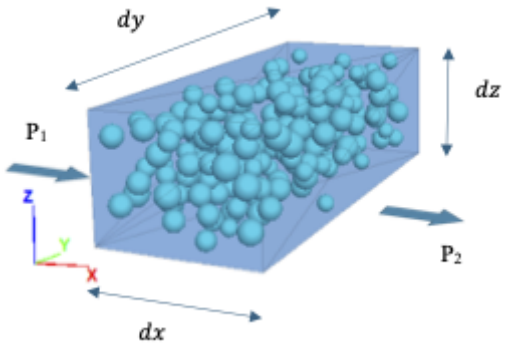

Figure 14. Small volume of propped fracture subjected to fluid flow.

This expression holds for both proppant and fine particles. The gradient of pressure is here the average computed in the cell where the particle (or center of the particle for the large ones) stands.

4.3.1. Influence of the solid particles on the fluid flow

The influence of the solid particles on the fluid flow relates directly to the relationship between the quantity of particles present in a finite volume cell and the average permeability of the cell. In the standard implementation available in PFC3D, this is provided by the classical Kozeny–Carman expression:

$$K(\epsilon) = \frac{1}{180}\frac{\epsilon^3}{(1-\epsilon)^2}d_p^2 \tag{8}$$

where d_p is an effective diameter of the particles defined by [Carrier, 2003]. This expression has the advantage of being very simple, it is a one-to-one relationship between the porosity and the local intrinsic permeability. It has also a severe drawback for the present application: if the particles inside a cell are in motion, they are still accounted for in the calculation of the permeability, although they should not alter the fluid flow in the cell in the limit case where the particle velocity is exactly that of the fluid velocity. This drawback can be solved by devising a modified permeability model.

The new expression of the permeability relies on a "Darcy-Poiseuille" modelling principle. Let us consider the equilibrium of a small volume of propped fracture subjected to a gradient of pressure $\Delta P = P_1 - P_2$, see Figure 14:

$$(P_1 - P_2)S = (\Delta P_{pois})V + \sum F_{particles/fluid} \tag{9}$$

where S is the area of the cross section subjected to the fluid flow, V the volume considered $V = S.\mathrm{d}x$, ΔP_{pois} is the force due to Poiseuille flow in the volume without the particles and $F_{particles/fluid}$ the forces due to the presence of the particles that oppose to the fluid flow, i.e. drag forces. The pressure is assumed to be constant in a finite volume cell and buoyancy forces are neglected.

In the finite volume cell, and on average, Darcy's law is assumed to hold:

$$\vec{v} = -K\mu\vec{\nabla}P_{darcy} \tag{10}$$

where K is the darcy's permeability of the cell containing the particles and in the cell without particle, it is Poiseuille law which holds:

$$\vec{v} = -\frac{k_p}{\mu}\vec{\nabla}P_{pois} = \frac{h^2}{12\mu}\vec{\nabla}P_{pois} \tag{11}$$

where h is the fracture opening, μ is the dynamic viscosity of the fluid and k_p the Poiseuille's permeability. Equation (9) can be re-written as:

$$\vec{\nabla}P_{darcy}\mathrm{d}xS = \sum \vec{F}_{drag} + \vec{\nabla}P_{pois}.\mathrm{d}xS \tag{12}$$

where the forces due to the particles on the fluid are the drag forces expressed in Equations (4) to (6). Substitution of Equations (10) and (11) into this equation yields:

$$\frac{\vec{v}\mu}{K}\mathrm{d}xS = \sum \vec{F}_{drag} + \frac{\vec{v}\mu}{k_p}\mathrm{d}xS \tag{13}$$

from which the apparent permeability K_{eff} of the cell can be obtained:

$$\frac{1}{K_{eff}} = \frac{\|\sum \vec{F}_{drag}\|}{\|\vec{v}\|\mu V} + \frac{1}{k_p} \tag{14}$$

In this expression, it can be noted that: (i) if the particles are moving at the same velocity of the fluid, then the permeability reduces to Poiseuille permeability. If particles are moving at a slower speed compared to the fluid, drag forces increase and the permeability decreases. If the particles are not moving at all, it turns out that the permeability is quite close to that obtained according to the Kozeny–Carman formula, as we will see next.

4.4. Comparisons with experiments

Before we start, it should be underlined that the exact configuration of the experiments is not reproduced: we deal with an axial fluid flow (on average) in a rectangular fracture instead of a radial flow (on average) in a penny shape fracture. This is merely for computational size reasons as the model runs on a standard desktop computer.

Trends and orders of magnitude of permeability should be considered only. Obtaining numerical results that are consistent with experiments informs on the basic mechanisms driving the unclogging process induced by the dynamic stimulation.

One should keep in mind that the computational model is very small compared to the expected size of fractures. In a large fracture, the unclogging process is much more complex. Particles that are put in motion due to the dynamic stimulation may find themselves trapped farther e.g., if they are blocked due to the variation of crack aperture, to clusters of fine particles that are not moving, or if the stimulation is attenuated and may no longer sustain the particle motions. Concluding on the efficiency of dynamic stimulation for practical applications calls for computations on large fractures that would be compared to on site experiments eventually.

In this paper, a single frequency and a single amplitude of the signal have been used, along with a single quantity of fine particles (15 %). The frequency is 10 Hz and the amplitude is 5.4 MPa. Results will highlight the effect of the proppant size distribution and density at constant amplitude and frequency. They are, however, informative with respect to

Table 3. Evolution of the permeability due to the dynamic stimulation (half a layer of proppant 40/70, 15 % of fines).

Permeability (m^2)	Clean propped fracture	Clogged fracture	Clogged fracture after stimulation
Experiments	$1.39 \cdot 10^{-10}$	$4.88 \cdot 10^{-11}$	$6.61 \cdot 10^{-11}$
Computations	$4.80 \cdot 10^{-10}$	$6.84 \cdot 10^{-11}$	$1.17 \cdot 10^{-10}$

two mechanisms: the destabilization of clusters of fine particles and the motion of proppant particles. A thorough comparison, covering the influence of the frequency and amplitude of the dynamic signal is left for future studies.

Let us first consider the case of propped fractures where the fine particles have reached the equilibrium and formed clusters. Figure 15 shows the evolution of the apparent permeability for two layers of proppant (30/50 and 40/70). We have reported here the results of computations performed with the two permeability models. The best agreement is obtained according to the Kozeny–Carman permeability model but the permeability values estimated by the two numerical models are of the same order of magnitude as those measured in experimental tests.

The dynamic stimulation has been applied with a percentage of fine particles of 15 %. First, proppant size 40/70 is considered with a quantity of particles corresponding to half a layer (see experimental results in [Fawaz et al., 2021]). Figure 16 shows the clogged propped fracture before and after the dynamic stimulation. Due to the stimulation, clusters of fine particles have moved, allowing for a larger apparent permeability. Also, proppant particles have moved during the stimulation. This can be observed by comparing the location of proppant particles in Figure 16 a and b. Table 3 shows the evolution of permeability due to stimulation. The computation results provide trends that are similar to the experimental data.

The same computation has been performed with two layers of proppant 40/70. Figure 17 shows the fracture before and after the dynamic stimulation. On this figure, the clusters of fine particles are shown in black and the proppant particles are shown in blue. Compared to Figure 17, one can see that when the proppant density is increased, the number of clusters of fine particles increases too. Again, one can observe on Figure 17 that fine particles have moved during the stimulation. After the stimulation, a cluster of fine particles has formed at the bottom right of the fracture (circled in red). This is better observed in Figure 18 where the distribution of the local permeability is shown before and after the dynamic stimulation. These observations underline the fact that during the stimulation, clusters may be destabilized, and then formed again elsewhere. 48 % of the fine particles have been evacuated outside the fracture. This is consistent with experimental observations showing that 30 % to 60 % of the fine particles are evacuated outside the specimen.

Table 4. Evolution of the permeability due to the dynamic stimulation (two layers of proppant 40/70, 15 % of fines).

Permeability (m^2)	Clean propped fracture	Clogged fracture	Clogged fracture after stimulation
Experiments	$4.86 \cdot 10^{-11}$	$1.08 \cdot 10^{-11}$	$3.4 \cdot 10^{-11}$
Computations	$5.50 \cdot 10^{-11}$	$1.20 \cdot 10^{-11}$	$1.01 \cdot 10^{-10}$

Table 5. 5 Evolution of the permeability due to the dynamic stimulation (two layers of proppant 30/50, 15 % of fines).

Permeability (m^2)	Clean propped fracture	Clogged fracture	Clogged fracture after stimulation
Experiments	$7.17 \cdot 10^{-11}$	$2.64 \cdot 10^{-11}$	$6.17 \cdot 10^{-11}$
Computations	$1.45 \cdot 10^{-10}$	$6.00 \cdot 10^{-11}$	$1.30 \cdot 10^{-10}$

Table 4 shows that the initial and final values of permeability computed according to the numerical model are again similar to those observed in the experiments. Table 5 shows the result of the same calculation with proppant 30/50. Trends correspond again to what is observed experimentally. The recovery of permeability is greater with proppant 30/50 than that with proppant 40/70. As expected, the computational model is capable to capture the relative effect of the size of the proppant particles compared to that of fine particles. At this time, we have not performed computations with a larger number of fine particles as they become rapidly very much computationally extensive. Also, it should be underlined that the number of pulses needed to reach unclogging is one order of magnitude less that observed in experiments. This may be due to the axial configuration of the fluid flow compared to experiments, and to the size of the fracture which is smaller in the computations compared to the experiments.

5. Conclusions

Dynamic stimulation of the propped fractures helps to increase their permeability. Here we show through this experimental study carried out on fractures filled with two layers of proppant, the influence of the proppant particle size, fines content, amplitude and frequency of the dynamic signal.

The tests performed with the proppant 40/70 show recovery rates that vary between 7 and 69 %. This rate rises to 9-100 % for tests performed with the proppant 30/50. A better recovery is observed when the size of the proppant particles increases. This is because pore sizes increase with the diameter of the proppant particles. Also, results highlight the role of the relative size of the proppant and fine particles. Fines

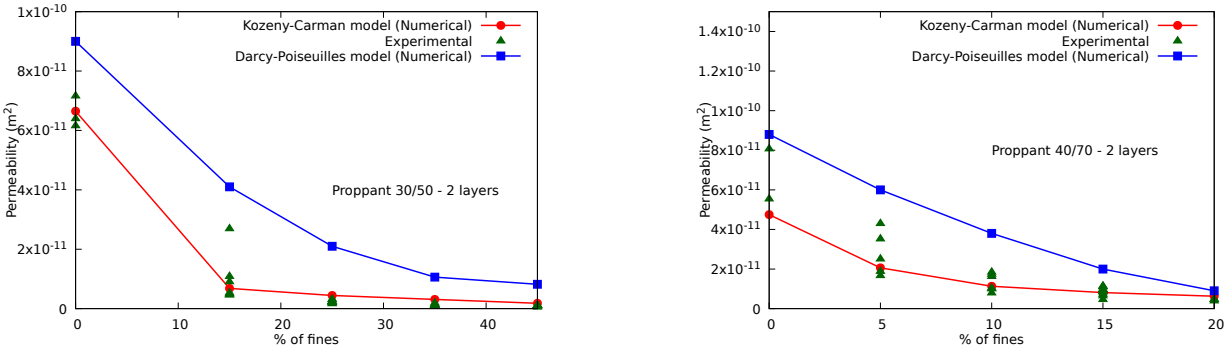

Figure 15. Evolution of the permeability with the percentage of fine particles: clogged fractures with two layers of different proppants (30/50 - left and 40/70 – right).

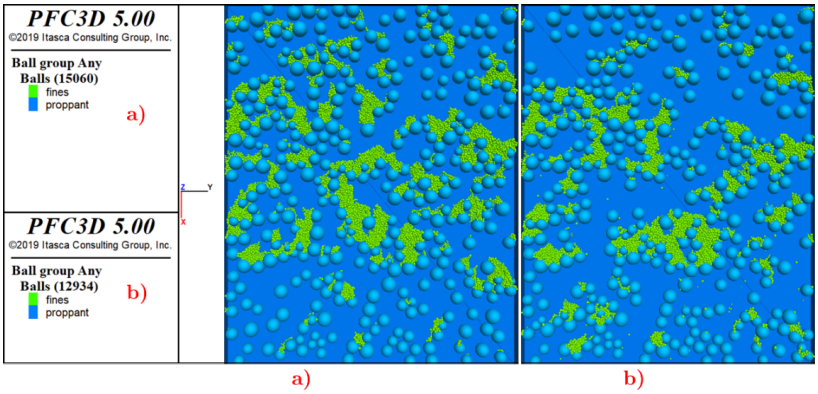

Figure 16. Distribution of particles before (a) and after (b) the dynamic stimulation. The fluid flow is downward. The fracture is filled with half a layer of proppant 40/70 and 15 % of fines

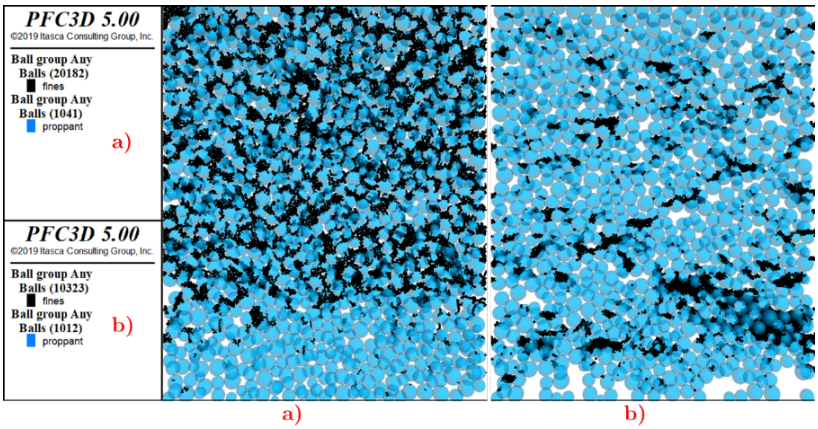

Figure 17. Distribution of particles before (a) and after (b) the dynamic stimulation. The fluid flow is downward. The fracture is filled with two layers of proppant 40/70 and 15 % of fines.

whose diameter is larger than the hydraulic pore size, cannot be released during the dynamic stressing and the unclogging process cannot take place. This was observed on the case of a fracture filled with two layers of 40/70 proppant and clogged with 20 % fines.

As for the influence of the dynamic stimulation, low frequencies have higher efficiency when the fractures are poorly clogged. It is the number of pulses setting the particles in motion that seems important in this case. High frequencies seem to be more efficient to unclog highly clogged fractures. High frequencies are most useful to destabilize numerous clusters of fine particles. The effect of the amplitude seems mostly related to the motion of proppant particles. The larger the amplitude, the greater the possibility of moving proppant particles.

A coupled (staggered) DEM/finite volume model has been used to get some insight on the basic phenomena that drive the increase of permeability during dynamic stimulation. Taken separately, the DEM and fluid models are classical, it is the coupled effects that required attention.

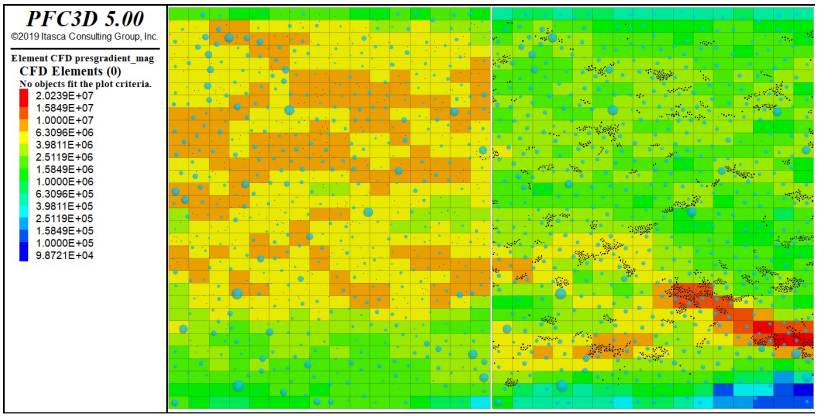

Figure 18. Distribution of permeability in the fracture before (left) and after the stimulation. Case of two layers of proppant 40/70 with 15 % of fines.

The Kozeny–Carman formula provides a first approximation relating the fluid fraction in the cell to the permeability. This model, however, fails when particles inside the finite volume cells are in motion. A new permeability model, which account for this effect has been presented. In substance, if the velocity of the particles is equal to that of the fluid phase, the permeability follows a standard Poiseuille model.

Computations have been performed on small, propped fractures with two quantities and sizes of proppant. Uniaxial fluid low is considered. They show a reasonable agreement with experimental data on the permeability of clean fractures, clogged fractures, and stimulated fracture. Computations confirms that the fine particles and the proppant particles are put into motion during the dynamic stimulation. Results show that the increase in fracture permeability is correlated to the motion of the proppant particles. For the geometry of the computational model considered in this study, it is the motion of proppant particles which seems to be the most important factor that break clusters of fine particles, allowing the flow of fines and unclogging.

It should be underlined that further simulations, performed on representative geometries are needed to confirm the above conclusion. The observed influence of the frequency and amplitude of the dynamic stimulation needs also to be corroborated with computational results especially. The potential application of this technique on a field pilot has been considered and discussed in a sequel to this study [Fensky et al., 2022], and this fracture stimulation method remains to be tested on the field to prove its efficiency.

Conflicts of Interest

The authors declare that there is no conflict of interest. The complete review history is available online.

Acknowledgements

The authors would like to thank TotalEnergies E&P at CSTJF, Pau for its financial and diligent support of this project. We also acknowledge the partial financial support of the Investissement d'Avenir French program (ANR-16-IDEX-0002) under the framework of the E2S hub-UPPA Newpores. Itasca consulting-Lyon is also acknowledged for their help and assistance in the numerical work.

References

Bedrikovetsky, P., Vaz, A., Machado, F., Zeinijahromi, A., and Borazjani, S. (2012). Skin Due to Fines Mobilization, Migration, and Straining During Steady-State Oil Production. *Petroleum Sci. Technol.*, 30(15):1539–1547.

Bennion, D. B. (2002). An Overview of Formation Damage Mechanisms Causing a Reduction in the Productivity and Injectivity of Oil and Gas Producing Formations. *J. Can. Petroleum Technol.*, 41(11).

Beresnev, I. A. and Johnson, P. A. (1994). Elastic-wave stimulation of oil production: A review of methods and results. *Geophysics*, 59(6):1000–1017.

Beresnev, I. A., Vigil, R. D., Li, W., Pennington, W. D., Turpening, R. M., Iassonov, P. P., and Ewing, R. P. (2005). Elastic waves push organic fluids from reservoir rock. *Geophys. Res. Lett.*, 32(13).

Candela, T., Brodsky, E. E., Marone, C., and Elsworth, D. (2014). Laboratory evidence for particle mobilization as a mechanism for permeability enhancement via dynamic stressing. *Earth Planet. Sci. Lett.*, 392:279–291.

Candela, T., Brodsky, E. E., Marone, C., and Elsworth, D. (2015). Flow rate dictates permeability enhancement during fluid pressure oscillations in laboratory experiments. *J. Geophys. Res. Solid Earth*, 120(4):2037–2055.

Carrier, W. D. (2003). Goodbye, Hazen; Hello, Kozeny-Carman. *J. Geot. Geoenv. Eng.*, 129(11):1054–1056.

Chen, G., Ewy, R. T., and Yu, M. (2010). Analytic solutions with ionic flow for a pressure transmission test on shale. *J. Petroleum Sci. Eng.*, 72(1–2):158–165.

Di Felice, R. (1994). The voidage function for fluid-particle interaction systems. *Int. J. Multiphase Flow*, 20(1):153–159.

Economides, M. J. and Nolte, K. G., editors (2000). *Reservoir stimulation*. Wiley & Sons, 3rdd ed. edition. Includes bibliographical references and index.

Elkhoury, J. E., Niemeijer, A., Brodsky, E. E., and Marone, C. (2011). Laboratory observations of permeability enhancement by fluid pressure oscillation of in situ fractured rock. *J. Geophys. Res.*, 116(B2).

Fawaz, Y., La Borderie, C., Sénéchal, P., Jacques, A., and Pijaudier-Cabot, G. (2021). Fracture cleaning: Experimental study on the unclogging process within a propped fracture under a dynamic stimulation. *J. Petroleum Sci. Eng.*, 206.

Fensky, C., Fawaz, Y., Perri, M., Borderie, C., Pijaudier-Cabot, G., and Jacques, A. (2022). Rejuvenate Unconventional Wells by Application of High Pression Pulse Waves in the Fracture Network – An Alternative to Refracturing Operations. In *Proceedings of the 10th Unconventional Resources Technology Conference*, URTeC 2022. American Association of Petroleum Geologists.

Guyer, J. E., Wheeler, D., and Warren, J. A. (2009). FiPy: Partial Differential Equations with Python. *Comput. Sci. & Eng.*, 11(3):6–15.

Itasca (2018). Pfc — Particle Flow Code V5.0.

Kang, Y., Xu, C., You, L., Yu, H., and Zhang, B. (2014). Comprehensive evaluation of formation damage induced by working fluid loss in fractured tight gas reservoir. *J. Nat. Gas Sci. Eng.*, 18:353–359.

Manga, M., Beresnev, I. A., Brodsky, E. E., Elkhoury, J. E., Elsworth, D., Ingebritsen, S. E., Mays, D. C., and Wang, C. (2012). Changes in permeability caused by transient stresses: Field observations, experiments, and mechanisms. *Rev. Geophys.*, 50(2).

Nikolaevskiy, V. N., Lopukhov, G. P., Liao, Y., and Economides, M. J. (1996). Residual Oil Reservoir Recovery With Seismic Vibrations. *SPE Prod. & Facilities*, 11(02):89–94.

Reinicke, A., Rybacki, E., Stanchits, S., Huenges, E., and Dresen, G. (2010). Hydraulic fracturing stimulation techniques and formation damage mechanisms—Implications from laboratory testing of tight sandstone–proppant systems. *Geochemistry*, 70:107–117.

Roberts, P. M. (2005). Laboratory observations of altered porous fluid flow behavior in Berea sandstone induced by low-frequency dynamic stress stimulation. *Acoust. Phys.*, 51(S1):S140–S148.

Xu, B. H. and Yu, A. B. (1997). Numerical simulation of the gas-solid flow in a fluidized bed by combining discrete particle method with computational fluid dynamics. *Chem. Eng. Sci.*, 52(16):2785–2809.

Xu, C., Kang, Y., You, Z., and Chen, M. (2016). Review on formation damage mechanisms and processes in shale gas reservoir: Known and to be known. *J. Nat. Gas Sci. Eng.*, 36:1208–1219.

Manuscript received 3rd June 2022, revised 3rd November 2023 and 17th January 2024, accepted 22nd January 2024.